

RAY-TRACING OPTIONS TO MITIGATE THE NEUTRAL ATMOSPHERE DELAY IN GPS

Felipe G Nievinski and Marcelo C. Santos

Geodetic Research Laboratory, Department of Geodesy and Geomatics Engineering
University of New Brunswick, Fredericton

One of the most rigorous way of quantifying the neutral atmosphere radio propagation delay is with ray-tracing, i.e., supposing the signal to be a ray and tracing its path, from satellite to receiver. We demonstrate how one can find significant discrepancies in ray-traced neutral atmosphere delays, due to reasonable variations in the underlying models. We offer a three part contribution. The first part is the separation of the ray-tracing options into three orthogonal groups: atmospheric source, atmospheric structure, and ray-path model. The second contribution is the systematization of model alternatives within each group, namely, atmospheric sources made of climate models, radiosondes, and numerical weather models; the atmospheric structures called spherical concentric, spherical osculating, ellipsoidal, gradient, and 3d; and the ray-path models bent-3d, bent-2d, straight-line, and zenithal. The third part of this contribution is the experimental comparison of these different models, in which we quantified the resulting discrepancy in terms of delay. Our findings are as follows. (i) Regarding ray-path models, the bent-2d model, albeit not strictly valid in a 3d atmosphere, introduces only negligible errors, compared to the more rigorous bent-3d model (in a 15-km horizontal resolution atmospheric model). Regarding atmospheric structures, we found that (ii) the oblateness of the Earth cannot be neglected when it comes to predicting the neutral atmosphere delay, as demonstrated by the poor results of a spherical concentric atmosphere; (iii) the spherical osculating model is the only one exhibiting azimuthal symmetry; (iv) the oblateness of the Earth is adequately accounted for by a spherical osculating model, as demonstrated by the small discrepancy between a spherical osculating and a more rigorous ellipsoidal model; and (v) a gradient atmosphere helps in accounting for the main trend in azimuthal asymmetry exhibited by a 3d atmosphere, but there remains secondary directions of azimuthal asymmetry that only a full 3d atmosphere is able to capture.

La façon la plus rigoureuse de quantifier le délai de propagation radioélectrique de l'atmosphère neutre est peut-être celle du tracé du rayon, c'est-à-dire en présupposant que le signal est un rayon et en reconstituant son parcours, du satellite au récepteur. Nous démontrons la façon de trouver des écarts importants dans les délais d'atmosphère neutre par tracé de rayon, dus à des variations raisonnables dans les modèles sous-jacents. Nous offrons une contribution en trois parties. La première partie est la division des options de tracé du rayon en trois groupes orthogonaux : la source atmosphérique, la structure atmosphérique et le modèle de parcours des rayons. La deuxième est la systématisation de modèles de remplacement au sein de chaque groupe, notamment les sources atmosphériques constituées de modèles climatiques, de radiosondes et de modèles météorologiques numériques; les structures atmosphériques appelées concentriques sphériques, osculatrices sphériques, ellipsoïdales, gradient, 3d; et les modèles de parcours de rayon fléchi-3d, fléchi-2d, en ligne droite et zénithale. La troisième partie de cette contribution est la comparaison expérimentale de ces trois modèles distincts dans laquelle nous quantifions les écarts qui en résultent en termes de délais. Nos conclusions sont les suivantes : (i) en ce qui a trait aux modèles de parcours de rayon, le modèle fléchi-2d, même s'il n'est pas strictement valide dans une atmosphère 3d, présente uniquement des erreurs négligeables comparativement au modèle fléchi-3d plus rigoureux (dans un modèle atmosphérique de résolution horizontale de 15 km). En ce qui a trait aux structures atmosphériques, nous avons conclu que (ii) l'aplatissement de la Terre ne peut pas être négligé lorsqu'il s'agit de prévoir le délai d'atmosphère neutre, comme le démontrent les résultats mitigés d'une atmosphère concentrique sphérique; (iii) le modèle d'osculatrice sphérique est le seul qui présente une symétrie azimutale; (iv) l'aplatissement de la Terre est correctement pris en compte par un modèle d'osculatrice sphérique, comme le démontre le faible écart entre une osculatrice sphérique et un modèle ellipsoïdal plus rigoureux; et (v) un gradient atmosphérique permet de tenir compte de la tendance principale de l'asymétrie azimutale présentée par une atmosphère 3d, mais il reste des directions secondaires de l'asymétrie azimutale que seule une atmosphère entièrement 3d peut saisir.



Felipe G. Nievinski
f.nievinski@unb.ca



Marcelo C. Santos
msantos@unb.ca

1. Introduction

As the radio signals emanating from GPS satellites propagate through the Earth’s electrically neutral atmosphere, they suffer *refraction*. Refraction affects the signal velocity in two ways: the signal speed is retarded and the signal direction gets bent. If not adequately mitigated, refraction corrupts estimates obtained from GPS observations collected at a particular epoch, receiver position, and satellite direction. One of the most rigorous way of quantifying the neutral atmosphere radio propagation delay is with *ray-tracing*, i.e., supposing the signal to be a ray and tracing it along its path, from satellite to receiver. In the present work we demonstrate how one can find significant discrepancies in ray-traced neutral atmosphere delays, due to reasonable variations in the underlying models.¹

Ray-tracing requires the creation or adoption of an atmospheric model; pragmatically, it can be interpreted as a function, having as argument or input an epoch and a position (corresponding to a point along the ray-path), and returning as output the pressure, temperature, and humidity at that point. We distinguish between two aspects making up a more comprehensive atmospheric model: structure and source. Atmospheric structure is a label for the arrangement of the iso-indicials;² for example, if the index of refraction is constant along spherical shells, we speak of a spherical atmospheric structure. Atmospheric source, on the other

hand, denotes the origin of the data making up the atmospheric model (such as radiosondes) or the purpose in generating that atmospheric model (such as weather or climate modeling).

We offer a three-part contribution. The first part is the separation of the ray-tracing options into three groups—atmospheric source, atmospheric structure, and ray-path model—each represented as an axis in Figure 1. The second one, detailed in section 2, is the identification of model alternatives within each group, listed along each axis in Figure 1. The third part of this contribution in section 3, is the experimental comparison of different models, in which we quantified the resulting discrepancy in terms of delay.

The diagram of ray-tracing options (Figure 1) deserves additional explanation. The options are ordered along each axis with the simplest ones closer to the origin and the more rigorous farther away from the origin. As we shall see later, simpler options approximate more rigorous ones sufficiently well over common and useful special cases. Furthermore, the possibility of mixing options from different groups is a good opportunity to validate more complicated models, comparing them to simpler ones at the cases for which we expect no discrepancy. This ordering was particularly fruitful in enabling the identification of previously unknown models, such as the ellipsoidal atmospheric structure. Notice also that the orthogonality in the diagram axes implies that alternative models compete only within the same group and not with models from a different group. This disentangles aspects that are typically lumped together, in a statement such an “this raytracer assumes spherical symmetry”, which actually makes separate claims about the aspects of ray-path and atmospheric structure. Certainly some combinations that are more common, but here we propose that such a choice be made and communicated more explicitly.

2. Models

Hereafter, we adopt the following notation: [Torge 2001] geodetic coordinates (latitude φ , longitude λ , geodetic height h , also known as ellipsoidal height), global Cartesian coordinates (roughly speaking³, having origin at the centre of mass of the Earth, X axis pointing towards the intersection of the Greenwich meridian with the equator, Z axis pointing towards the north pole, and Y axis in such a way that it completes a right-handed system), and local

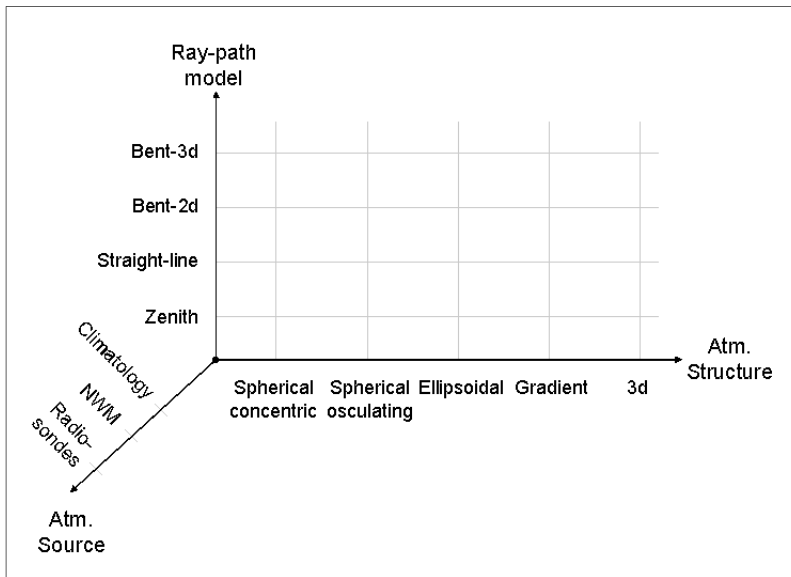


Figure 1: Diagram of options available in ray-tracing.

¹ For implementation and numerical aspects, please see *Nievinski* [2009, Appendix I].

² An iso-indicial is a surface of constant refractivity or index of refraction.

³ The precise definition is laid down in *McCarthy and Petit* [2004].

Cartesian coordinates (x axis pointing towards the east direction, y axis pointing towards the north direction, and z axis pointing upwards, along the ellipsoidal normal). The function denoted as $\frac{XYZ}{\varphi\lambda h}$ () converts from geodetic to global Cartesian coordinates. Position vectors such as \mathbf{r} are assumed expressed in global Cartesian coordinates, i.e., $\mathbf{r} = X\hat{\mathbf{I}} + Y\hat{\mathbf{J}} + Z\hat{\mathbf{K}}$; when we need position vectors in local Cartesian coordinates we will indicate that as $\mathbf{r}^{xyz} = x\hat{\mathbf{i}} + y\hat{\mathbf{j}} + z\hat{\mathbf{k}}$. Elevation angle ε is always reckoned from the ellipsoidal horizon or, equivalently, zenith angles are always reckoned from the ellipsoidal normal.

2.1 Ray-Path Models

In this section we discuss different models for the shape, scale, position, and orientation of the ray-path.

First of all we must recognize that when we speak about the electromagnetic signal as a ray we have implicitly adopted the framework of classical geometrical optics. It implies that we assume the wavelength of the radiation under study to be negligibly small compared to the extent of the perturbations in the medium of propagation. In other words, we assume that the atmosphere is nearly uniform at spatial distances comparable to that wavelength, roughly speaking. Consequently, under that theory we are unable to account for effects such as diffraction and scattering.

The ray-path, in its general form, is a 3d curve. In propagation media with special structure (section 2.2), though, it assumes simpler shapes. For example, in a spherical atmosphere (sections 2.2.1 and 2.2.2), the ray-path degenerates into a plane curve, i.e., it is contained on a plane, as shown in section 2.1.2. As another example, if the ray's tangent direction always coincides with the gradient of refraction in a medium, then the ray degenerates further, into a straight-line, as described in section 2.1.4; the straight-line case, albeit not always rigorously valid, is a good approximation for most of the sky of a ground-based receiver, as we discuss in section 2.1.3.

2.1.1 Bent-3d

The most general ray-path model is defined by the fundamental equation of classical geometrical optics, the *Eikonal equation* [Born and Wolf 1999]:

$$\frac{d}{dl} \left(n \frac{d\mathbf{r}}{dl} \right) = \nabla n \quad (1)$$

This differential equation describes the *change* in the ray position vector \mathbf{r} along the ray-path. We see that it depends critically on the propagation medium: n is the (scalar) field of index of refraction and ∇n is its gradient (vector) field.⁴ The actual position $\mathbf{r}(l)$ at any given distance l along the ray-path depends on both the propagation medium and a set of conditions. A common choice of initial conditions are an initial position and an initial direction, in which case the final position is determined from eq. (1). A common choice of boundary conditions are initial and final positions, in which case the initial direction is determined from eq. (1).⁵

2.1.2 Bent-2d

In an atmosphere with spherical structure the gradient of refractivity ∇n always points to the centre of the sphere:

$$\hat{\nabla} n = \frac{\nabla n}{|\nabla n|} = -\hat{\mathbf{r}} = -\frac{\mathbf{r}'}{|\mathbf{r}'|}, \quad (2)$$

where $\mathbf{r}' = \mathbf{r} + \mathbf{r}_c$ is the position vector with respect to the centre of the (possibly osculating) sphere (section 2.2). The consequence of a null horizontal component in the gradient of refractivity is the absence of any out-of-plane bending in the ray-path. In other words, in an atmosphere exhibiting spherical structure the ray-path is rigorously a plane curve (hence the suffix “2d” in the name).

This model is embodied in the widely used Bouguer's formula [Born and Wolf 1999, p. 131]:

$$nr' \sin z = \text{const.}, \quad (3)$$

where $z = 90^\circ - \varepsilon$ is the zenith angle and r' is the distance to the centre of the (possibly osculating) sphere. Following Young [2006, p. 99–100] we can recast eq. (3) in the form of a differential equation:

$$dr' = -\tan(z) dn / n. \quad (4)$$

Equation (4) can be interpreted as a generalization of Snell's law:

$$n \sin \theta = (n + dn) \sin(\theta + d\theta), \quad (5)$$

where θ is the ray's angle of incidence with respect to the normal at the interface of two media.

In the actual Earth's atmosphere, the horizontal component, though not exactly null, is always

⁴ By field we mean that n and ∇n associate a value (scalar and vector, respectively) to any position in space, not only to positions along the ray-path.

⁵ The Eikonal as well as boundary conditions are discussed in detail in Nievinski [2009, Appendix I].

much smaller than its vertical counterpart, making the bent-2d a satisfactory approximation most of the time.

2.1.3 Straight-line

This model neglects any bending in the ray-path. It is defined as:

$$\mathbf{r} = \mathbf{r}_0 + l \hat{\mathbf{s}}_0, \quad (6)$$

where $\mathbf{r}_0 \stackrel{XYZ}{\leftarrow}_{\varphi\lambda h} (\varphi_0, \lambda_0, h_0)$ is the receiver position

vector; $\hat{\mathbf{s}}_0$ is the direction (a unit vector) from receiver to satellite; l is the usual along-path distance, except that now we postulate it to be equal to zero at the receiver and increasingly positive towards the satellite (equivalently, we could define the ray-path from the satellite to the receiver, instead).

The fact that the along-path distance incidentally equals the straight-line distance brings a tremendous advantage over preceding models (bent-3d, bent-2d), namely, that the entire (postulated straight-line) ray-path is known in advance. That is in contrast with models that allow for bending, in which the ray-path needs to be discovered step-by-step or iteratively. In numerical practice this means we need to solve a quadrature, instead of a differential equation. Although the straight-line may seem a crude approximation, it is satisfactory for a large portion of the sky, from zenith down to 30° in elevation angle. It was very common in early contributions [Saastamoinen 1972; Hopfield 1969].

2.1.4 Zenithal

This is a special case of both straight-line and bent-2d models, when the ray direction happens to coincide with the local vertical direction:

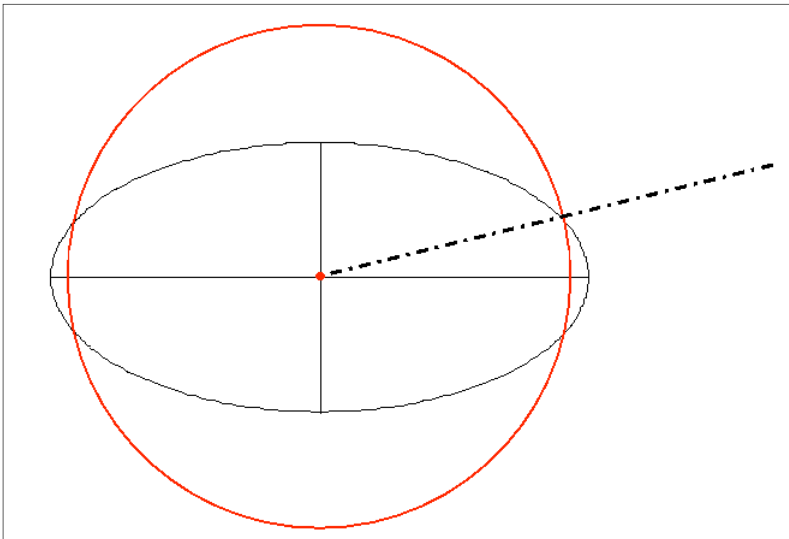


Figure 2: Sample spherical concentric iso-indicial (thick circle).

$$\mathbf{r} \stackrel{XYZ}{\leftarrow}_{\varphi\lambda h} (\varphi_0, \lambda_0, h_0 + l). \quad (7)$$

It is rigorously valid in an atmosphere with spherical osculating or ellipsoidal structure, and an excellent approximation in any structure. It is a very convenient form when one is interested in zenith delays only, because it allows one to simplify the path integrals to ordinary integrals having limits expressed in terms of height.

2.2 Atmospheric Structures

Atmospheric structure is a label for the arrangement of the iso-indicials in a given atmospheric model. For example, if the index of refraction is constant along spherical shells, we speak of a spherical atmospheric structure. In the present section we discuss the following atmospheric structures (from simplest to more elaborate): spherical concentric (section 2.2.1), spherical osculating (section 2.2.2), ellipsoidal (section 2.2.3), gradient (section 2.2.4), and 3d (section 2.2.5). Just like for the ray-path models, under atmospheric structure we have a general case (3d) and the remaining ones are simplifications of that general case, warranted by common and useful special cases.

The first four structures are profile-based, meaning that all the data they need are stored in the form of a single vertical profile, assumed the same for any horizontal position. In other words, vertical variation is modeled and horizontal variation is neglected. That is a good approximation to the Earth's atmosphere, in which, e.g., pressure decreases exponentially with increasing height. The differences among those four profile-based atmospheric structures lie in their subtle differences in the definition of horizontal coordinates, or, equivalently, of vertical coordinates. We make those definitions more clear and precise in the remainder of the present section.

Throughout this section, we will be using the form:

$$v = f(\dots),$$

where v stands for any of pressure, temperature, or humidity, and "... " will be replaced by the variables upon which the atmospheric parameters depend in each structure.

2.2.1 Spherical Concentric

In this model, illustrated in Figure 2, the vertical direction is defined coinciding with the radial direction of a sphere concentric with the Earth's centre of mass (or, more precisely, centred at the

origin of the global Cartesian coordinate system (X, Y, Z) , [McCarthy and Petit 2004]):

$$v = f(r), \quad (8)$$

where $r = |\mathbf{r}|$.

2.2.2 Spherical Osculating

This model takes the vertical direction as the radial direction of a sphere that osculates the ellipsoid at a particular base point. In such a case:

$$v = f(r'), \quad (9)$$

where $r' = |\mathbf{r}'|$ is the length of an eccentric position vector \mathbf{r}' :

$$\mathbf{r}' \equiv \mathbf{r} - \mathbf{r}_c,$$

The centre of the osculating sphere, \mathbf{r}_c is defined as:⁶

$$\mathbf{r}_c \stackrel{XYZ}{\leftarrow}_{\varphi\lambda h} (\varphi_0, \lambda_0, h_0 = -R);$$

the latitude φ_0 and longitude λ_0 specify the base point at which the sphere's radial direction coincides with the ellipsoid's normal direction; $R =$

\sqrt{MN} is the Gaussian radius of curvature;⁷ M, N are the radii of curvature along the meridian and prime vertical, respectively; the negative sign in $h = -R$ implies that the centre of the osculating sphere is located downward with respect to the ellipsoid's surface (Figures 3 and 4).

2.2.3 Ellipsoidal

This last profile-based atmospheric structure (Figure 5) takes the vertical direction as the ellipsoidal normal:

$$v = f(h), \quad (10)$$

which obviously yields a simple expression in terms of geodetic or ellipsoidal height h .

2.2.4 Gradient

The next approximation in terms of atmospheric structure may be described as a double-profile based model: we take the single profile exactly as defined for the ellipsoidal atmosphere (denoted here by v_0) and augment it with a second profile ($\nabla_H v_0$). Both profiles, v_0 and $\nabla_H v_0$, refer to a base location,

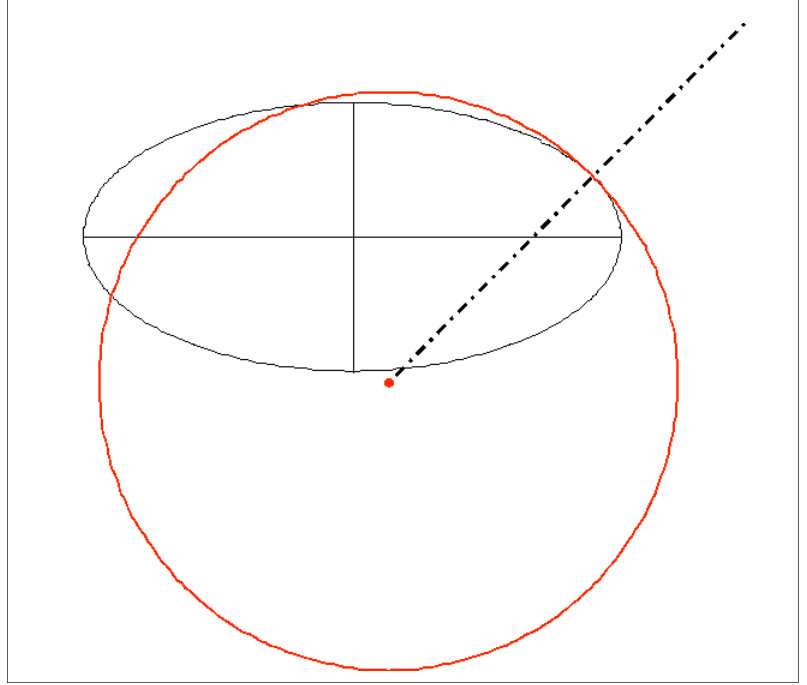


Figure 3: Sample spherical osculating iso-indicial (thick circle).

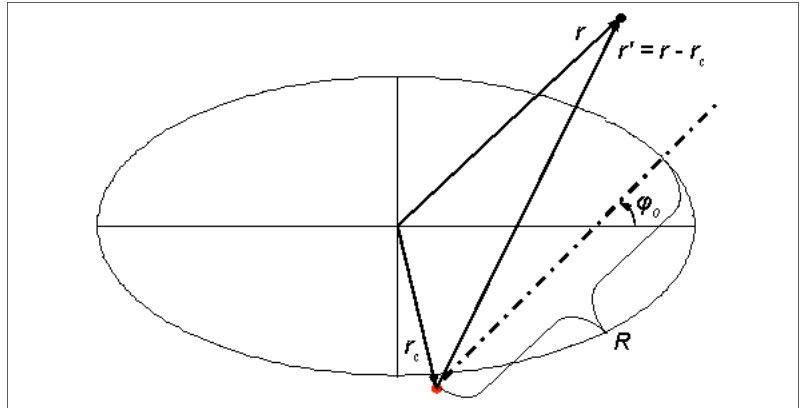


Figure 4: Angles, distances, and vectors involved in a spherical osculating atmosphere.

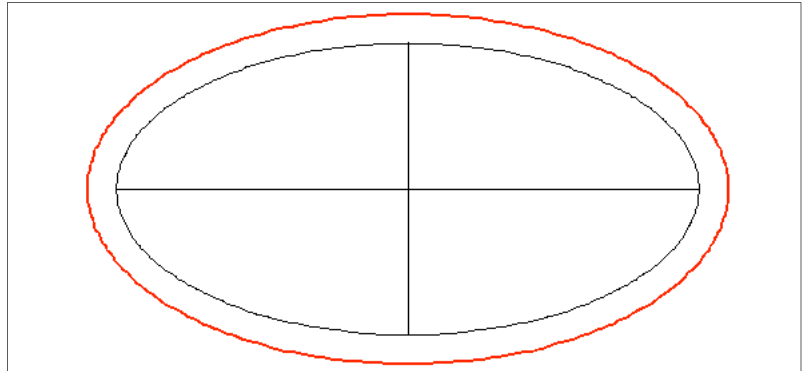


Figure 5: Sample ellipsoidal iso-indicial (thick, outer ellipsoid).

⁶ Please notice that $\mathbf{r}_c \stackrel{XYZ}{\leftarrow}_{\varphi\lambda h} (\varphi_0, \lambda_0, -R) \neq \mathbf{r}_0 \stackrel{XYZ}{\leftarrow}_{\varphi\lambda h} (\varphi_0, \lambda_0, h_0)$.

⁷ "An intrinsic property of the surface independent of the coordinate system used to describe that surface" [Weisstein 2008].

which is specified by φ_0, λ_0 (hence the subscript 0). We define the gradient atmosphere in such a way that there are possibly different values of mean v_0 and horizontal gradient $\nabla_H v_0$ for each different height h , but at any particular height h , v_0 and $\nabla_H v_0$ are the same for any horizontal position φ, λ , i.e.:

$$\begin{aligned} v_0 &= f(h), \\ \nabla_H v_0 &= f'(h). \end{aligned}$$

The resulting integrated v still depends on horizontal coordinates, though:

$$v = f(\varphi, \lambda, h) = f_0(h) + f_{\nabla_H}(\varphi, \lambda, h). \quad (11)$$

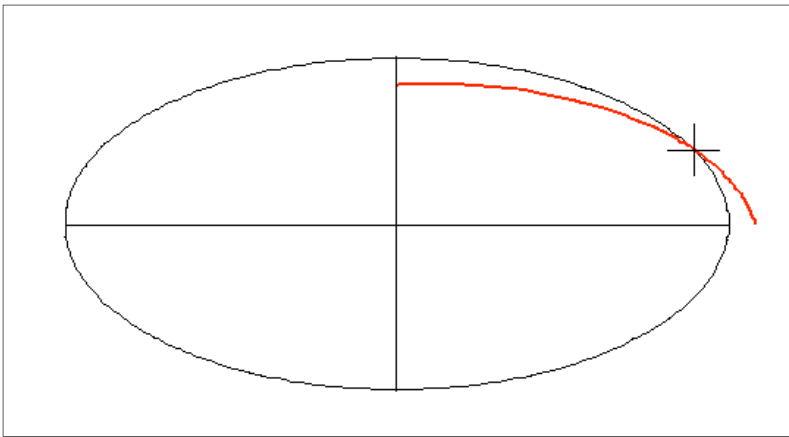


Figure 6: Sample gradient iso-indicial (thick line segment) in the vicinity of a base point (marked as a cross).

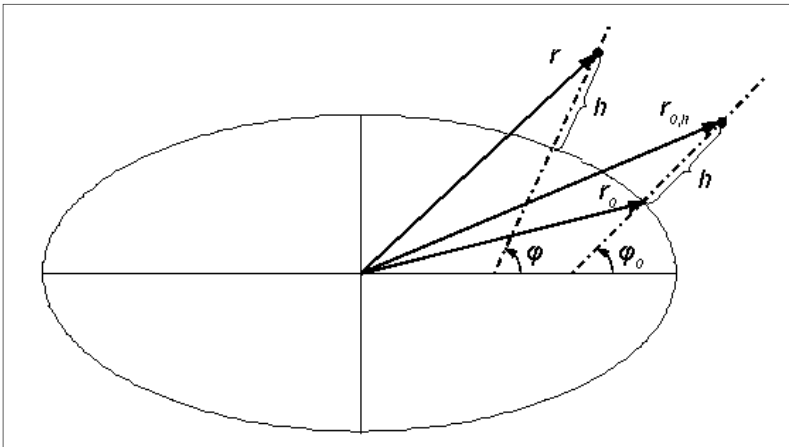


Figure 7: Angles, distances, and vectors involved in a gradient atmosphere.

⁸ Contrast (see also Figure 7):

$$\begin{aligned} \mathbf{r}_{\varphi\lambda h}^{XYZ} &\leftarrow (\varphi, \lambda, h), \\ \mathbf{r}_0^{\varphi\lambda h, XYZ} &\leftarrow (\varphi_0, \lambda_0, h_0), \\ \mathbf{r}_{0,h}^{\varphi\lambda h, XYZ} &\leftarrow (\varphi_0, \lambda_0, h). \end{aligned}$$

⁹ This is similar to the work presented by Gardner [1976], in the sense that $v_0, \nabla_H v_0$ are postulated constant with respect to horizontal coordinates but can change with height. The main difference is that, whereas Gardner employs a gradient for total refractivity, here we employ instead a gradient for each atmospheric parameter. Also Gardner builds his gradient atmosphere upon a spherical concentric atmosphere, whereas here we build it upon an ellipsoidal atmosphere. Finally, Gardner simplifies the equivalent of the integral in eq. (12) evaluating it along a geodesic (a spherical great circle in his spherical atmosphere), whereas we evaluate it along a loxodrome, the only path in which the horizontal gradient is rigorously constant.

The functions $f_0(h)$ and $f_{\nabla_H}(\varphi, \lambda, h)$ represent, respectively, the contribution from mean conditions and the horizontal gradient of the atmospheric parameter v . The former is exactly the same as the function defined for a single profile in an ellipsoidal atmosphere (section 2.2.3). The latter is:

$$f_{\nabla_H}(\varphi, \lambda, h) = \int_{r_{0,h}}^r \nabla_H v_0(\mathbf{r}) \cdot d\mathbf{r}. \quad (12)$$

where $\mathbf{r}_{\varphi\lambda h}^{XYZ}$ is the point of interest, at which

the atmospheric parameter v is sought; $\mathbf{r}_{0,h}^{\varphi\lambda h, XYZ}$ is a point lying along the normal passing through the base location, corresponding to the point of interest: it has the same vertical coordinate h as the point of interest \mathbf{r} but horizontal coordinates equal to the base location's (φ_0, λ_0) ⁸; “•” denotes the dot product.

The integral above can be performed along any path. There is one particular path, though, that simplifies to a closed-form expression: it is the path of constant azimuth, called a *loxodrome*. The resulting closed-form expression is:

$$f_{\nabla_H}(\varphi, \lambda, h) = l \left(\sin a \left. \frac{\partial v_0}{\partial x} \right|_h + \cos a \left. \frac{\partial v_0}{\partial y} \right|_h \right), \quad (13)$$

where $\partial v_0/\partial x$ and $\partial v_0/\partial y$ are directional derivatives of v along, respectively, east and north directions (thus making up the horizontal gradient), defined at the base location (φ_0, λ_0) and evaluated at a particular h ; l is the loxodrome length (which is not the same as the along-path distance l line distance), and a is the loxodrome azimuth (which is not the same as the azimuth of the initial ray direction, α); see Nievinski [2009, Appendix V] for details.⁹ Figures 6 and 7 illustrate the gradient atmospheric structure.

2.2.5 Three-Dimensional (3d)

This is the most general case: one makes no assumption about the variation of the atmospheric parameters, neither in the vertical nor horizontal directions. In other words, one takes as-is whatever the atmospheric source is able to represent (Figure 8).

2.3 Atmospheric Sources

In addition to atmospheric structure, there is another aspect making up a more comprehensive atmospheric model: atmospheric (model or data) source.

2.3.1 Radiosondes

The source constituted of radiosondes [Dabberdt *et al.* 2002] is the closest to reality, as they are actual observations. Usually the sensors are released from the ground hanging off a balloon, but sometimes they are dropped during flights hanging off a parachute, in which case they receive the name *dropsondes*. Their measurements have large vertical resolution (Figure 9) but have very small horizontal and time resolution: they are usually released from approximately 800 sites worldwide, twice daily.

It is interesting to notice that radiosondes, as used for predicting slant delays or slant factors, are not purely observations—they do require some modeling. First, height is not measured but rather derived, under the assumption of hydrostatic equilibrium, from the actual measurements of pressure, temperature, and humidity. Second, it requires interpolation among the vertically scattered measurements, for which one has to postulate a (linear, quadratic, log-linear, hydrostatic, etc.) model. Third, it requires interpolation for horizontal positions other than the launching sites' [Ghoddousi-Fard and Dare 2007; Ifadis and Savvaidis 2001], and even more dangerous, extrapolation beyond the coverage area of the ensemble of launching sites. Fourth, it requires interpolation and/or extrapolation at epochs other than the release epoch (which, by the way, is just a nominal value—the balloon takes up to a few hours to finish its course). Fifth, it requires a supplementary atmospheric model after the balloon bursts at its maximum height.

2.3.2 Numerical Weather Models

Another source to consider is that of numerical weather models (NWM) or, more precisely, their output [Lorenz 2002; Buizza 2002; Golding 2002]; see Figure 10. When that model output refers to a future epoch, one speaks of prediction; otherwise, analysis; which is the reason why we prefer to speak in general of a numerical weather model, regardless of whether it refers to a future or past epoch. Its output is a representation of the atmospheric fluid at specific instantaneous epochs. The representation includes a 3d field snapshot for each atmospheric parameter—pressure, temperature, humidity, amongst many others. It usually takes the form of

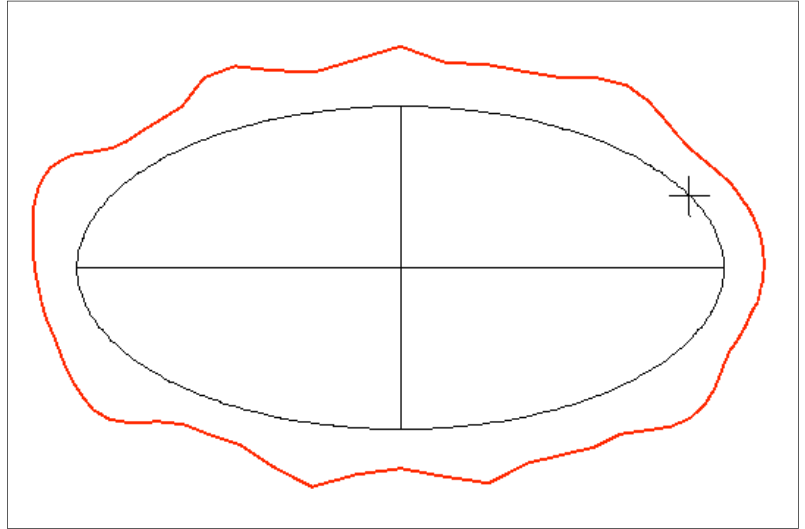


Figure 8: Sample 3d iso-indicial (thick, outer, jagged line).

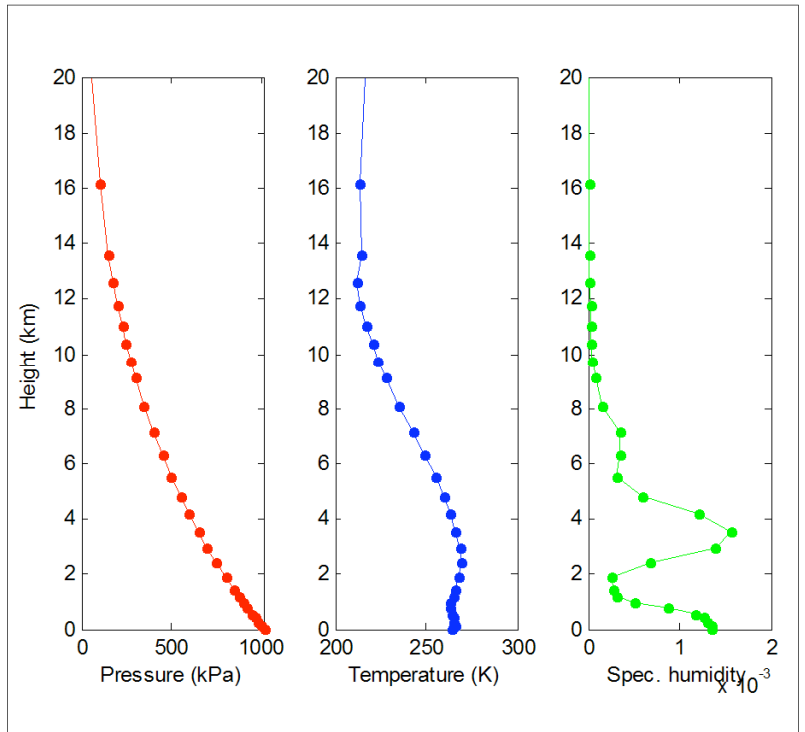


Figure 9: Sample radiosonde: vertical profile collected at a single site and epoch.

either an expansion in (volumetric) spherical harmonics or a discretization on a grid. Its main advantage over radiosondes is its much larger horizontal and time resolution. On the other side of the same coin there is the disadvantage of its large size (in bytes) requiring above-average digital equipment for storage and computations.¹⁰

¹⁰ For use in ray-tracing, a NWM usually needs to be supplemented with a climatology, because a NWM does not extend vertically as high as necessary.

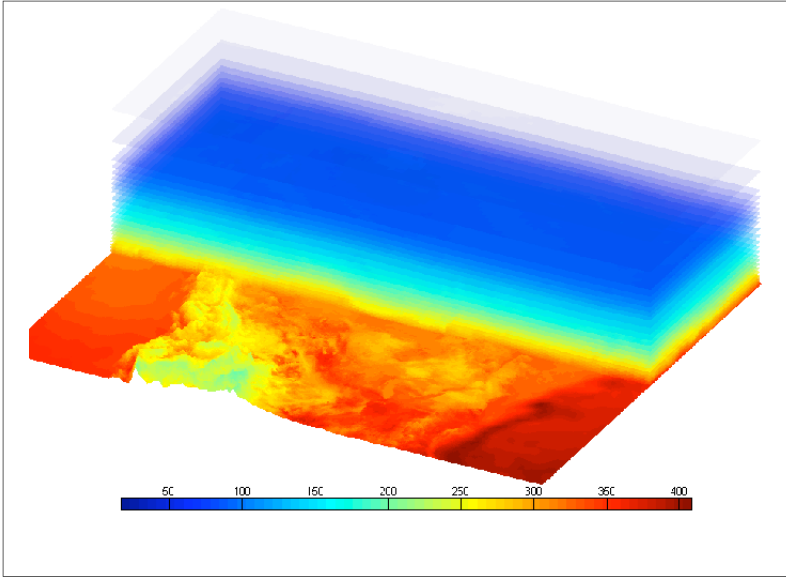


Figure 10: Sample numerical weather model: refractivity field (unitless) over North America on August 16, 2004 at 22:45 UTC, as given by the Canadian Regional Model [Côté et al. 1998] (vertical scale exaggerated 100x).

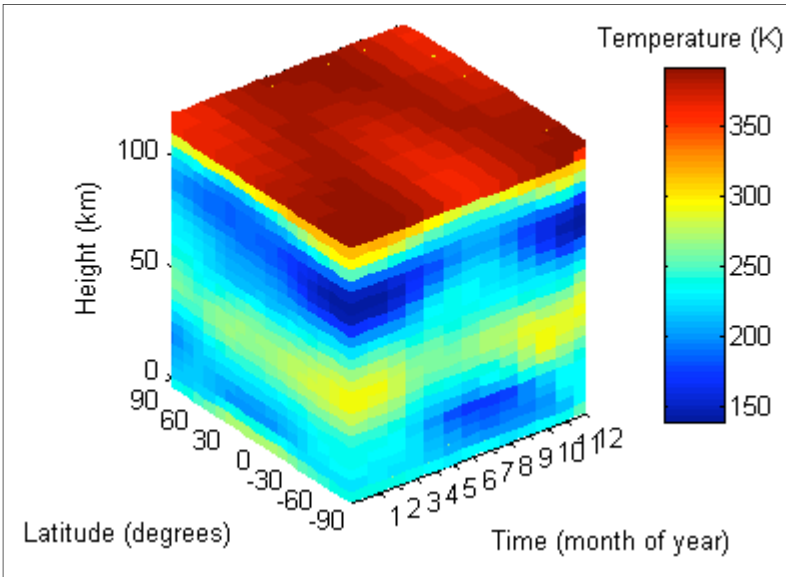


Figure 11: Sample climatology: temperature, as given by the CIRA86 model [Chandra et al. 1990; Fleming et al. 1988].

2.3.3 Climatologies

Yet another atmospheric source is that of climate models, or climatologies for short [Hartmann 2002]; see Figure 11. As the saying goes, climate is what we expect and weather is what we get. Consequently, a climatology will never be as good a source as a NWM, concerning the actual atmospheric conditions affecting GPS observations. Compared to radiosondes, climatologies are less

accurate, but radiosondes have a rather sparse area of coverage. The amount of discrepancy expected and the accuracy requirements for the intended GPS application will dictate which atmospheric source is better suited. Yet one particular climatology might be better than others.¹¹

3. Results

In the present section the most important combinations of ray-path and atmospheric structure are compared in terms of the resulting slant delay. The sequence of comparisons is summarized in Figure 12, where each arched arrow represents a pair-wise comparison. The atmospheric source is always fixed to NWM; more specifically, the Canadian regional weather model, which has a horizontal resolution of 15 km—we do expect the results to depend upon that resolution. Details about the ray-tracing procedure are given in Nievinski [2009, Appendix I]; results reported here were obtained with a tolerance of 0.1 mm.

We show the delay discrepancies in the form of a skyplot (e.g., Figure 13)—north is to the top, south is to the bottom, east to the right, and west to the left. Samples were taken at directions regularly spaced in azimuth (every 45°) and regularly spaced in $1 / \sin(\epsilon)$ (at 90°, 14°, 8°, 6°, 4°, 3°), which is approximately the way that the delay grows with elevation angle ϵ . The discrepancy in each of the delay components (namely, hydrostatic, non-hydrostatic, and geometric), in addition to the total, is shown separately; the sign of the discrepancies is depicted in different hues (blue for negative and red for positive), while the magnitude of the discrepancies is depicted both as the intensity of the colour and the radius of the balls at each sampled direction.

The delay discrepancies represent a snapshot, taken at a single epoch and location. The exact epoch and location (indicated in Table 1) were chosen to correspond to a near worst case scenario. That scenario is given by a category 4 hurricane, the 2004 Hurricane Charley.¹² The rationale for that choice was the understanding that, if we did not find significant discrepancies in such a scenario,

Table 1: Epoch and location of first experiment.

Epoch:	August 14, 2004, 12 h UTC
Latitude:	+33° 49' 01"
Longitude:	-76° 06' 28"

¹¹ For discussion, please see Mendes [1999, p. 48], Johnson et al. [2002], and Thessin [2005].

¹² 2004 Hurricane Charley was the strongest hurricane found within the spatial and time extents of our NWM archive.

then we should not expect anything worse under typical conditions.

3.1 Spherical Concentric vs. Spherical Osculating Atmospheres

The first thing to notice in the discrepancy between a spherical concentric and a spherical osculating atmosphere is its large magnitude, reaching metres and decimetres in the hydrostatic (Figure 13(a)) and non-hydrostatic (Figure 13(b)) components, respectively. The second aspect is a clear trend, in the north–south direction. We attribute the magnitude and trend of the discrepancy to the tilting of the spherical concentric horizon with respect to the spherical osculating horizon, as illustrated in Figure 14.

Figure 13 has important consequences with regard to azimuthal symmetry, i.e., whether a given atmospheric model yields the same delay values at the same elevation angle but different azimuths. At this point it should be apparent that at least one of the two spherical atmospheres is *not* azimuthally symmetric. In other words, a spherically symmetrical atmosphere does not necessarily translate into azimuthally symmetric delay. That is in contrast with the usage of those two expressions in the literature—it is not uncommon to find them being used interchangeably. Having checked both individually (see *Nievinski* [2009 p. 85]), we can assert that the spherical osculating one *is* azimuthally symmetric, while the spherical concentric one *is not*. A peculiar though perfectly admissible conclusion is that azimuthally symmetric mapping functions used in GPS processing are based on an osculating, not concentric, spherical atmosphere. This is dictated by the usage of a mapping function—regardless of its author’s intention or awareness when developing it—as a consequence of the practice of inputting elevation angles whose complement is reckoned from the ellipsoidal normal, rather than from the radial geocentric direction.

3.2 Spherical Osculating vs. Ellipsoidal Atmospheres

The discrepancies between a spherical osculating atmosphere and an ellipsoidal atmosphere, shown in Figure 15, have a much smaller magnitude than in the previous comparison; in fact, it is negligibly small in all but the hydrostatic component (Figure 15(a)). We also notice a clear trend: it reaches its maximum along the north–south direction, minimum along the east–west direction, and zero at the mid-directions. We attribute that trend to the fact that, whereas the radius of the osculating sphere is constant, $R = \sqrt{MN}$ (where M, N are the

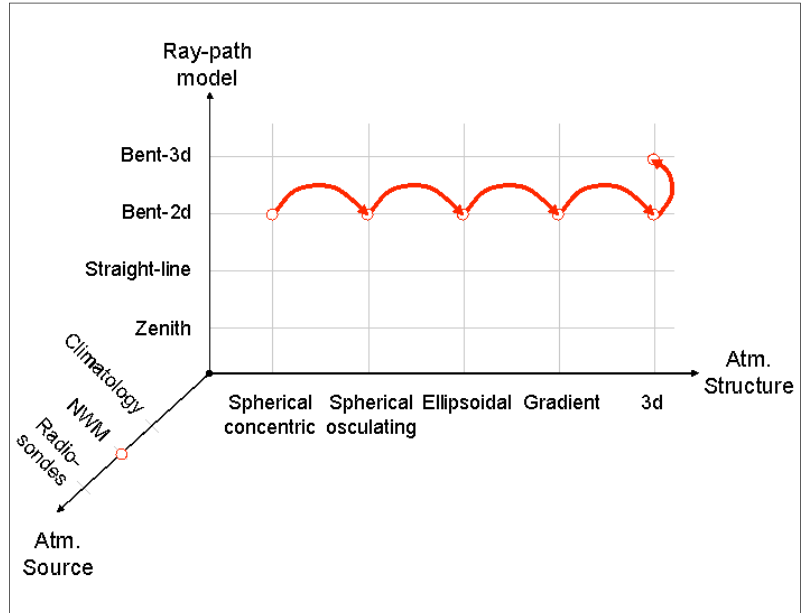


Figure 12: Diagram of sequence of pair-wise comparisons.

principal radii of curvature), the radius of curvature of the ellipsoid varies with azimuth:

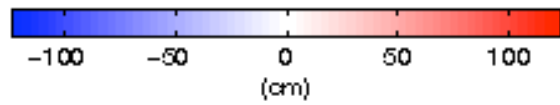
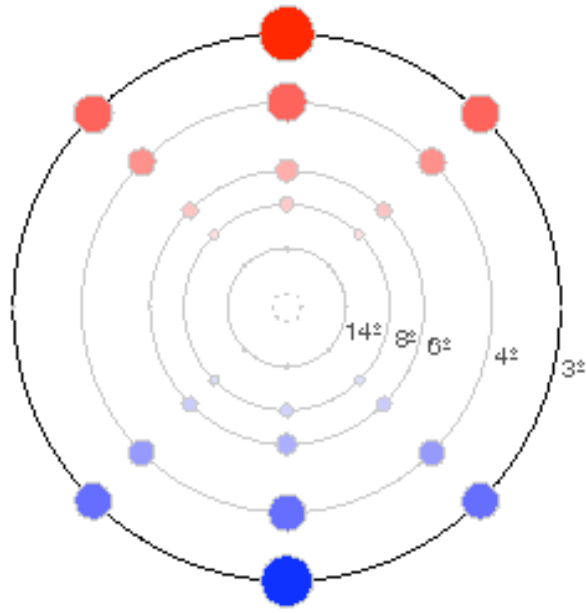
$$R_\alpha = \left(\frac{\cos^2 \alpha}{M} + \frac{\sin^2 \alpha}{N} \right)^{-1}.$$

In Figure 16 we show that the ellipsoidal shell is inside the spherical osculating shell along the north–south rhumb ($R < R_\alpha = M$), but it is outside along the east–west rhumb ($R > R_\alpha = N$), and the two surfaces intersect in between.

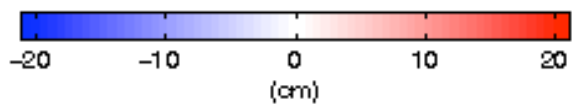
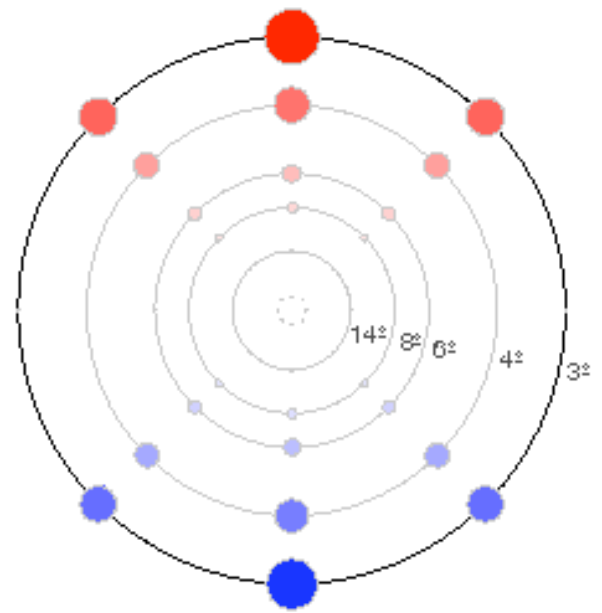
However small is the magnitude of the azimuthal asymmetry exhibited by an ellipsoidal atmosphere, the danger in neglecting it lies in the fact that it is a systematic effect. Therefore it will not be canceled out by data randomization (e.g., processing numerous days of GPS observations); rather, we expect it to persist thus biasing position estimates in an inescapable way.

3.3 Ellipsoidal vs. Gradient Atmospheres

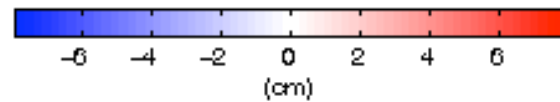
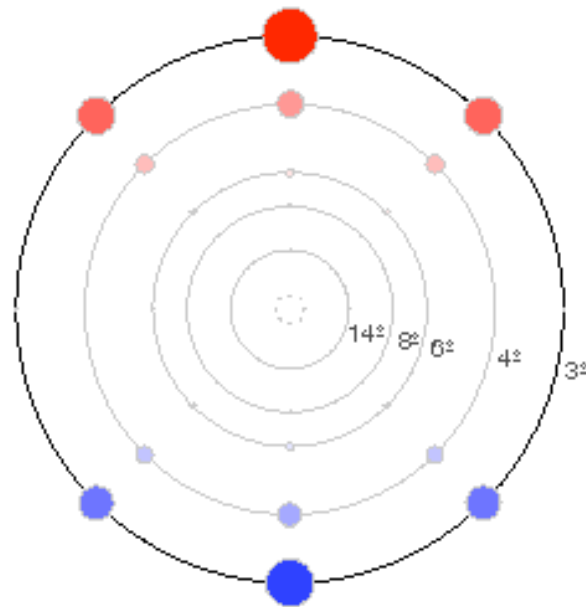
Please recall from section 2.2.4 that we allow for one independent horizontal gradient for each pressure, temperature, and humidity atmospheric field. Consequently, the azimuthal asymmetry exhibited in terms of delay may be more complex than a single main direction (e.g., SW–NE in Figure 17(a)) and may have different direction and magnitude in each delay component (contrast Figures 17(a) and 17(b)).



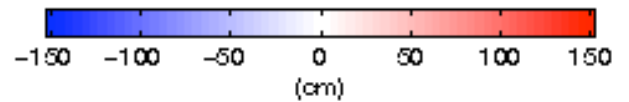
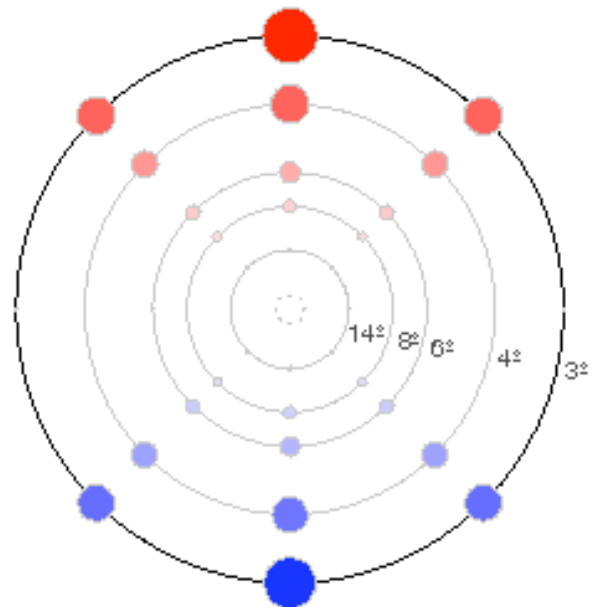
(a) Hydrostatic



(b) Non-hydrostatic



(c) Geometric



(d) Total

Figure 13: Results of first comparison: spherical concentric minus spherical osculating.

3.4 Gradient vs. 3d Atmospheres

Following the sequence summarized in Figure 12, the last comparison in terms of atmospheric structure is that between the gradient and 3d. First notice that the discrepancy (Figures 18(a) to 18(d)) tends to be smallest along the main direction previously represented by the gradient atmosphere (e.g., SW–NE in Figure 17(a)). That fact implies that the gradient atmosphere does a good job modeling the main direction of azimuthal asymmetry present in the 3d atmosphere. Nonetheless, there remains non-negligible, secondary directions of azimuthal asymmetry present in the 3d atmosphere that the gradient atmosphere is simply not able to capture.

The good agreement between gradient and 3d atmospheres along the main direction of azimuthal asymmetry intriguingly fails at the south portion of the skyplot. Notice how the south portion is significant in the gradient atmosphere (Figure 17(a) and does not cancel out in the discrepancy between gradient and 3d atmospheres (Figure 18(a)). That might be an indication that a local gradient taken at the base point might not be representative of the conditions too far away from the base point—at such low elevation angles the ray travels several hundred kilometres before exiting the neutral atmosphere (i.e., before it reaches a height of roughly 80 km).

3.5 Bent-2d vs. Bent-3d Ray-Path Models

Having finished the sequence of comparisons among different atmospheric structures, now we keep the atmospheric structure fixed to the most realistic one (3d), and then we compare the bent-3d and bent-2d ray-path models. What is most striking about their discrepancy, is the fact that the sum of the two along-path delays, hydrostatic (Figure 19(a)) and non-hydrostatic (Figure 19(b)), has nearly the same magnitude and opposite sign as the geometric delay (Figure 19(c)). As a consequence, when we add them together to make up the total (Figure 19(d)), they nearly cancel each other out.

We conclude that the small magnitude of the discrepancies shown in Figure 19 warrants the use of the simpler bent-2d ray-path model instead of the more complicated bent-3d one, even if used in conjunction with a 3d atmosphere that does contain horizontal gradients. Although admittedly a null result, it nevertheless saves future researchers from wasting effort in implementing these models. As a caveat, this conclusion is not necessarily valid with a NWM of higher horizontal resolution than the one we were using (15 km) and for ray-tracing studies interested in products other than the delay (e.g., bending angle).

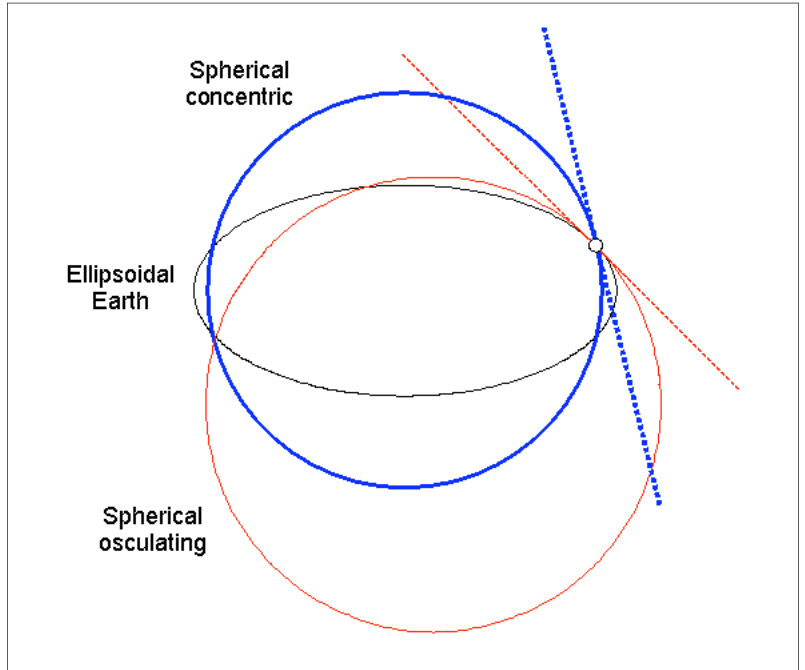


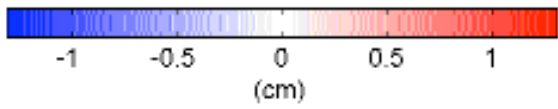
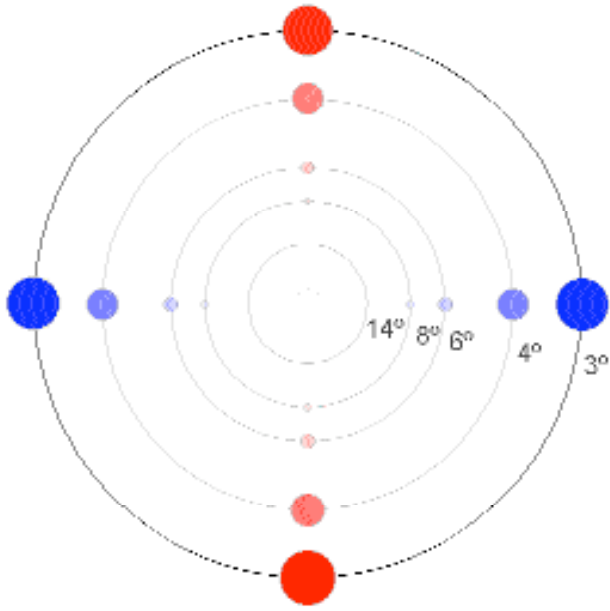
Figure 14: Horizons of each concentric (thick dotted line) and osculating (thin dotted line) spheres—base point is at $\varphi = 45^\circ$.

Inspecting the discrepancy in total delay more closely (Figure 19(d)), we notice that it is always positive (within the prescribed numerical integration tolerance), which means that the total delay given by the bent-2d ray-path model is always greater than that given by the bent-3d ray-path model. Therefore the ray always travels faster with the bent-3d model, a model that allows the ray to bend in whatever way the gradient of refraction directs, instead of forcing it to be a plane curve, as the bent-2d model does. In other words, the bent-3d model follows more closely Fermat's least time principle, in a 3d atmosphere. A similar rationale applies to a straight-line ray-path model (results not shown): the total delay given by a bent-2d ray-path model should always be smaller than that given by the straight-line ray-path, because even though ray bending obviously increases the geometric delay, it also decreases even more the along-path delay, resulting in a net decrease in total delay due to bending.

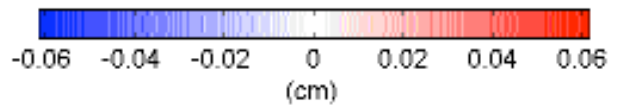
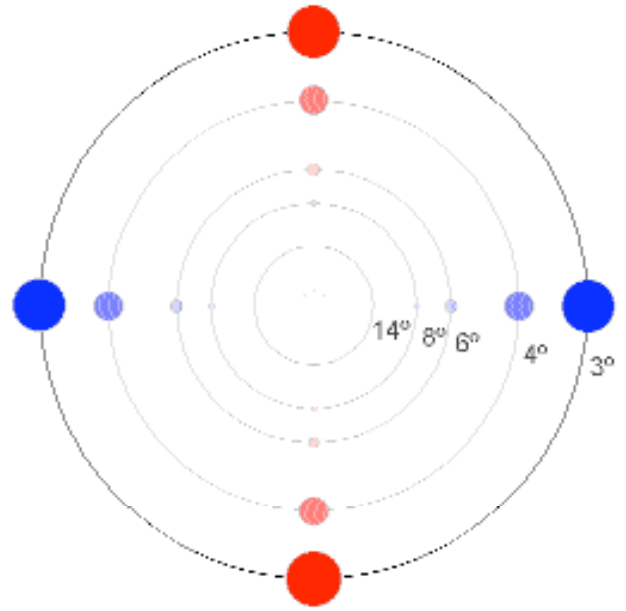
4. Conclusions and Future Work

We have demonstrated how one can find significant discrepancies in neutral atmosphere delays, due to reasonable variations in the models underlying ray-tracing.

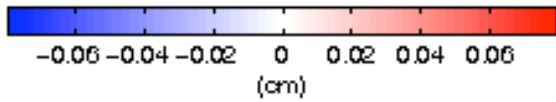
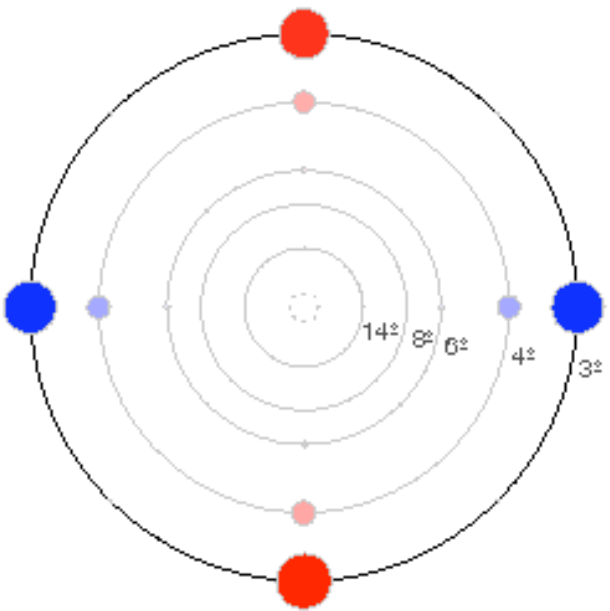
On the theoretical side, we introduced the distinction between atmospheric source, atmospheric structure, and ray-path model. We reviewed the existing atmospheric sources, namely, climate



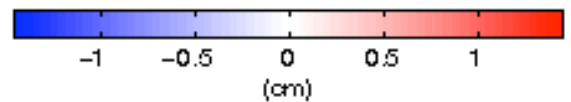
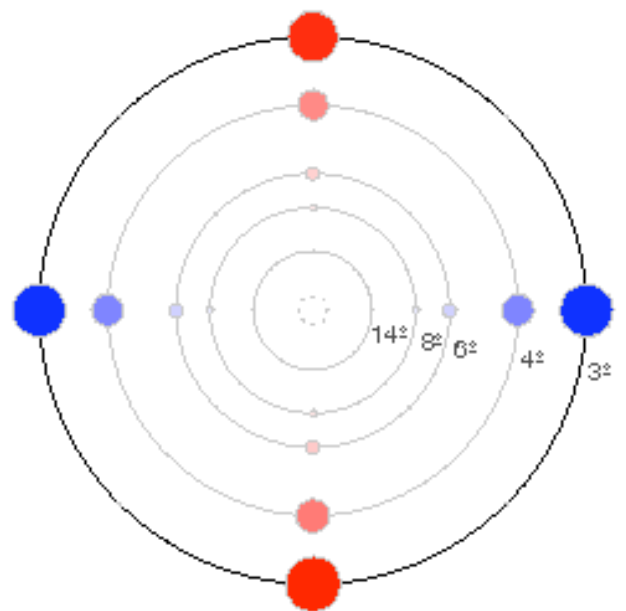
(a) Hydrostatic



(b) Non-hydrostatic



(c) Geometric



(d) Total

Figure 15: Results of second comparison: spherical osculating minus ellipsoidal.

models, radiosondes, and numerical weather models. We systematized the full range of atmospheric structures and ray-path models, from simplest to most rigorous. More specifically, we examined the atmospheric structures called spherical concentric, spherical osculating, ellipsoidal, gradient, and 3d; and the ray-path models bent-3d, bent-2d, straight-line, and zenithal.

On the experimental side, our findings were as follows. (i) Regarding ray-path models, the bent-2d model, albeit not strictly valid in a 3d atmosphere, introduces only negligible errors, compared to the more rigorous bent-3d model (in a 15-km horizontal resolution atmospheric model). Regarding atmospheric structures, we found that (ii) the oblateness of the Earth cannot be neglected when it comes to predicting the neutral atmosphere delay, as demonstrated by the poor results of a spherical concentric atmosphere; (iii) the spherical osculating model is the only one exhibiting azimuthal symmetry; (iv) the oblateness of the Earth is adequately accounted for by a spherical osculating model, as demonstrated by the small discrepancy between a spherical osculating and a more rigorous ellipsoidal model; and (v) a gradient atmosphere helps in accounting for the main trend in azimuthal asymmetry exhibited by a 3d atmosphere, but there remains secondary directions of azimuthal asymmetry that only a full 3d atmosphere is able to capture.

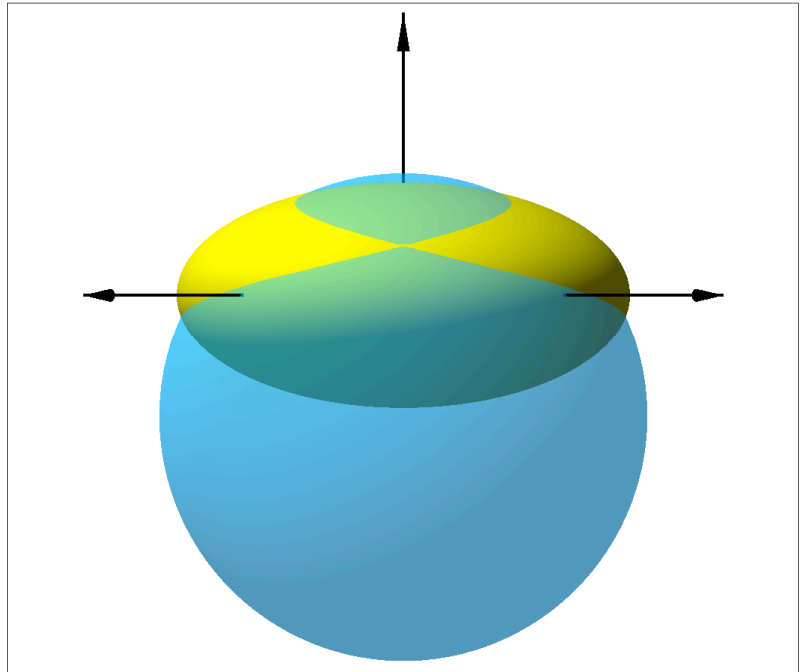
As for next steps, we are investigating the impact of such different models in the positioning domain; work is underway to perform the necessary GPS processing over sufficiently long time series and large geographical extents.

Acknowledgments

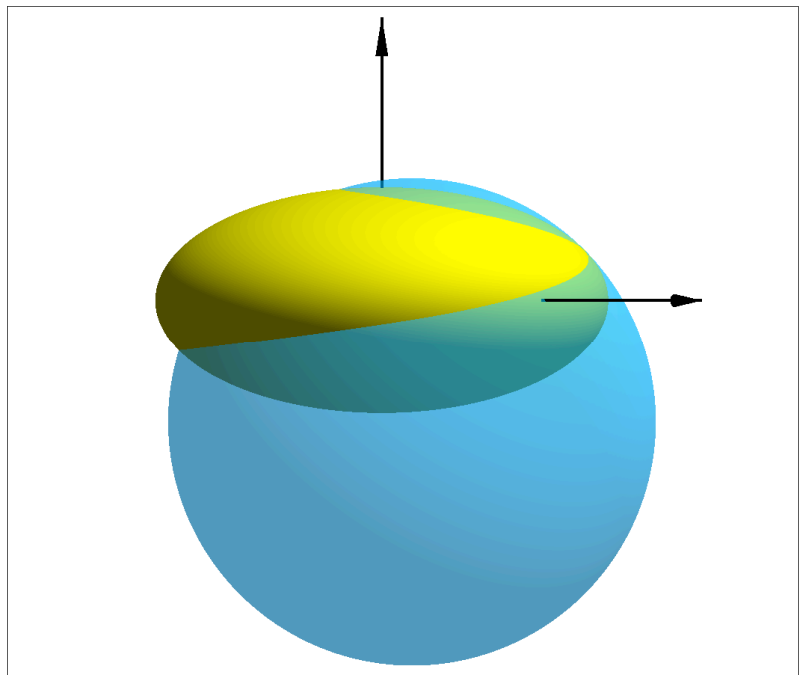
We acknowledge funding provided by CIDA, the Canadian International Development Agency; GEOIDE, Geomatics for Informed Decisions Network of Centres of Excellence; and NSERC, Natural Sciences and Engineering Research Council of Canada. Additionally, the Weather Office at Environment Canada is acknowledged for granting us access to the numerical output from the Canadian Regional Global Environmental Multiscale numerical weather model.

References

- Born, M., and E. Wolf. 1999. *Principles of Optics: Electromagnetic Theory of Propagation, Interference and Diffraction of Light*. 7th ed., 986 pp., Cambridge University Press, Cambridge, U.K., ISBN 0521642221, doi:10.2277/0521642221.
- Buizza, R. 2002. Weather prediction: Ensemble prediction. In *Encyclopedia of Atmospheric Sciences*, eds. J.R.



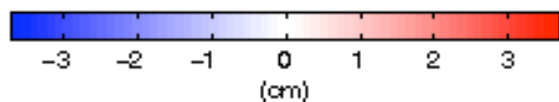
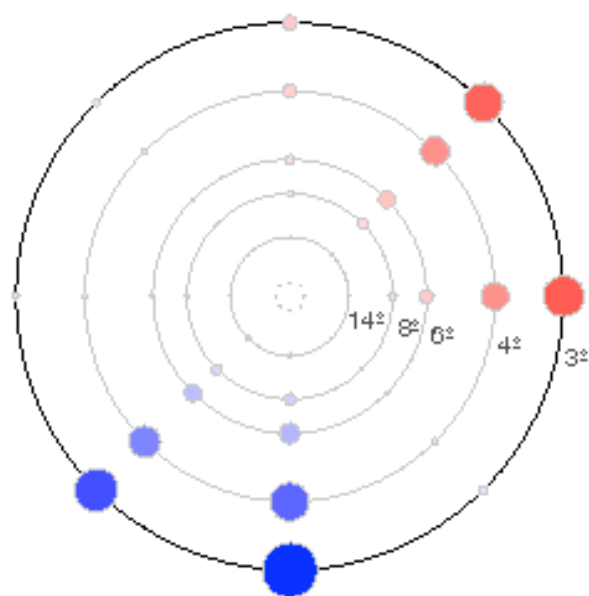
(a) Frontal view.



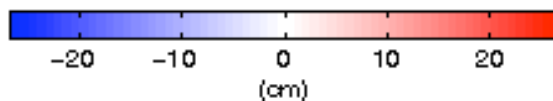
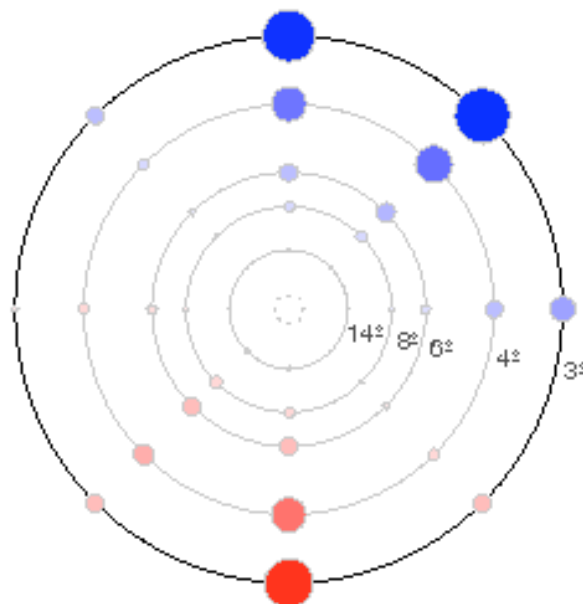
(b) Side view (see Figure 3 for the corresponding cross-section).

Figure 16: Constant radius of osculating sphere (larger, transparent shell) vs. azimuth-varying radius of ellipsoid (smaller, opaque shell); base point is at $\varphi = 45^\circ$, $\lambda = 45^\circ$; arrows represent axes of global Cartesian coordinate system (X, Y, Z).

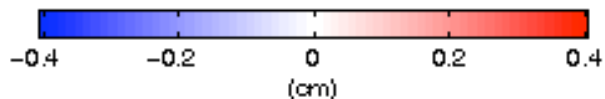
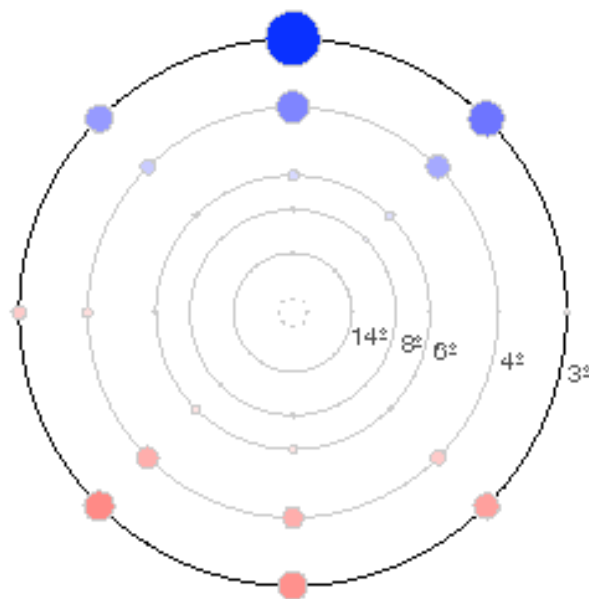
- Holton, J.A. Curry, and J.A. Pyle, Academic Press, Oxford, ISBN 9780122270901, pp. 2546–2557, doi:10.1016/B0-12-227090-8/00461-9.
- Chandra, S., E.L. Fleming, M.R. Schoeberl, and J.J. Barnett. 1990. Monthly mean global climatology of temperature, wind, geopotential height and pressure



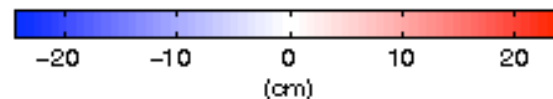
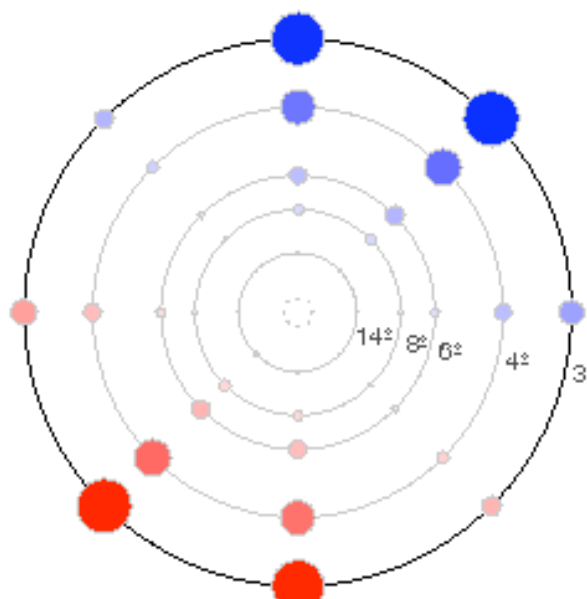
(a) Hydrostatic



(b) Non-hydrostatic

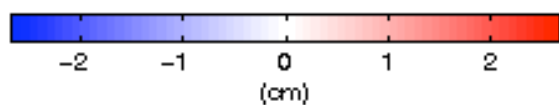
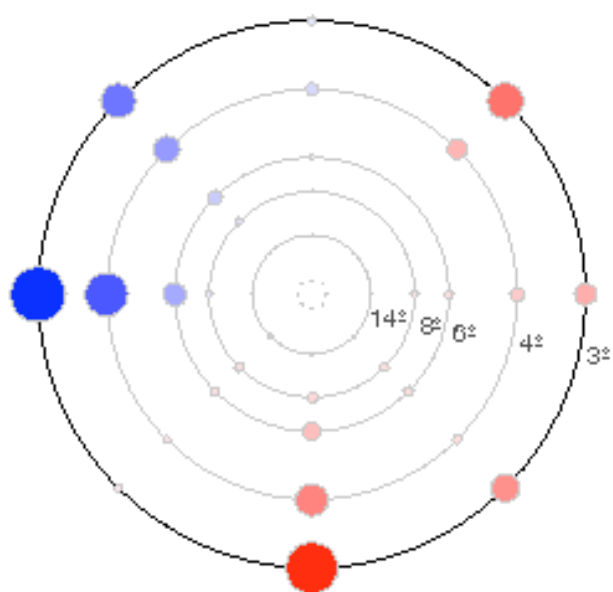


(c) Geometric

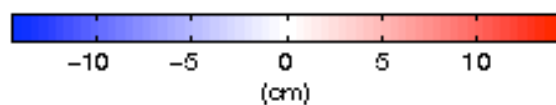
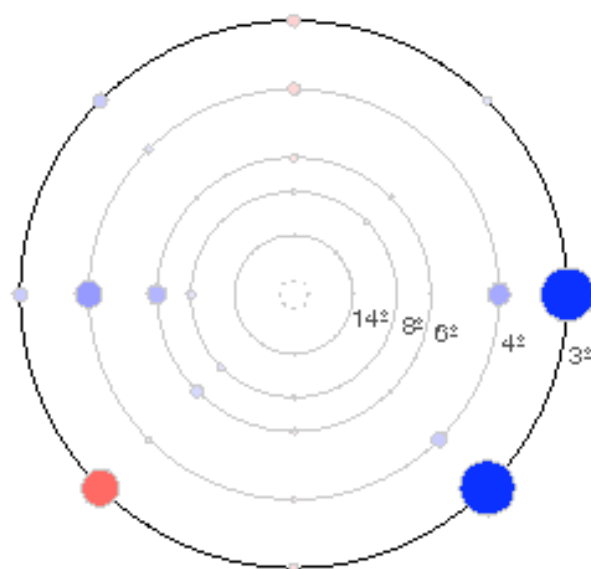


(d) Total

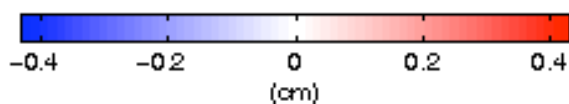
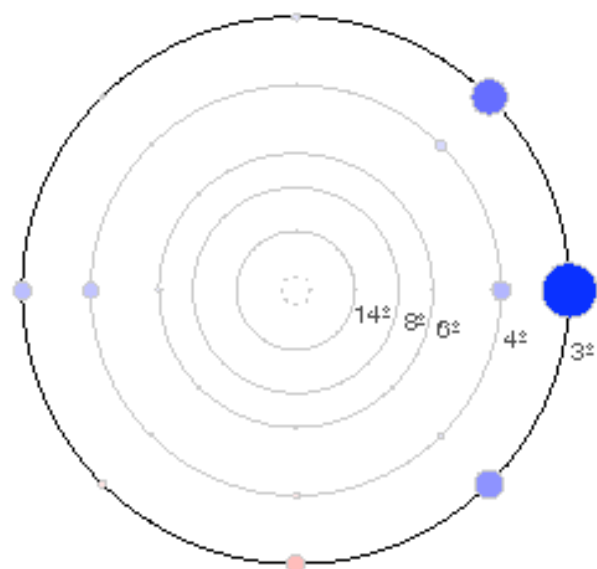
Figure 17: Results of third comparison: ellipsoidal minus gradient.



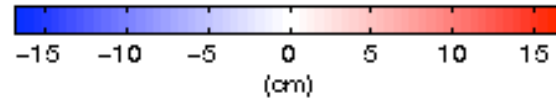
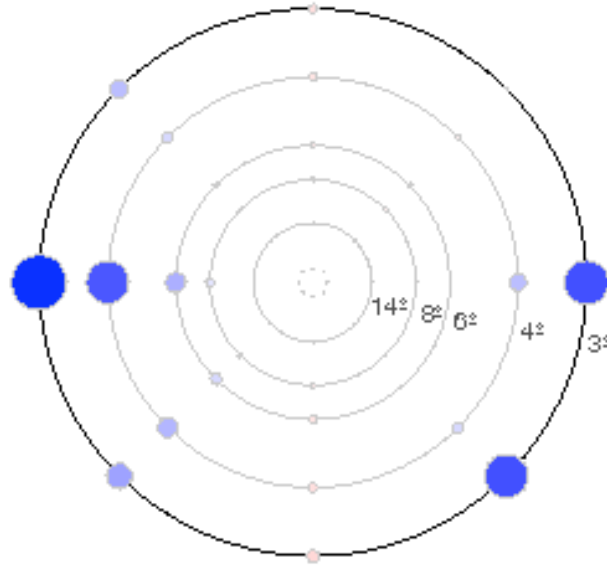
(a) Hydrostatic



(b) Non-hydrostatic

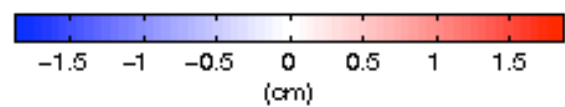
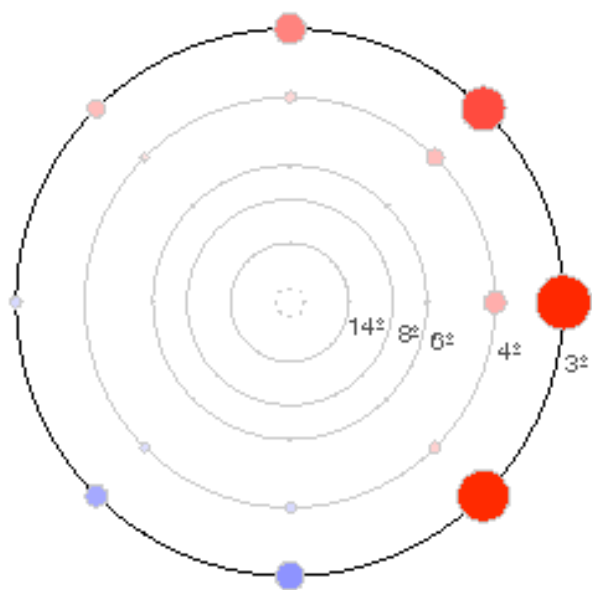


(c) Geometric

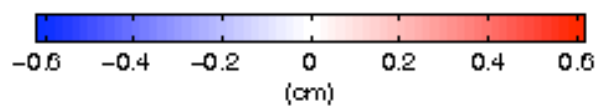
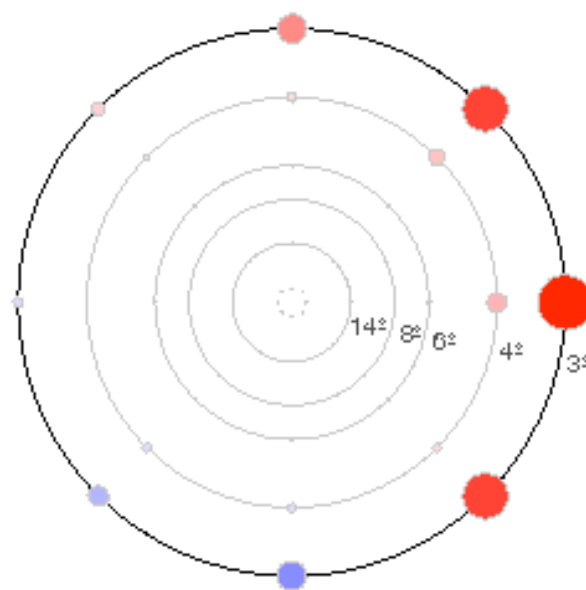


(d) Total

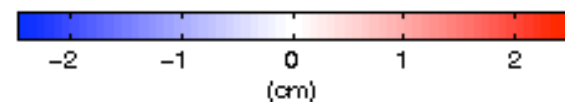
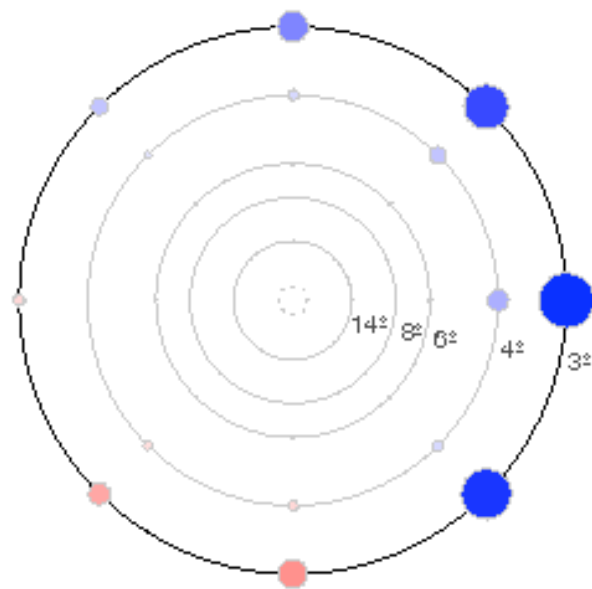
Figure 18: Results of fourth comparison: gradient minus 3d.



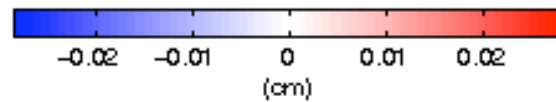
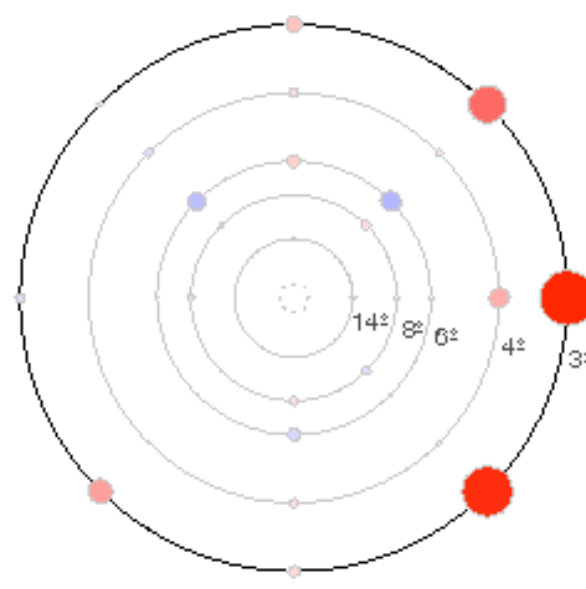
(a) Hydrostatic



(b) Non-hydrostatic



(c) Geometric



(d) Total

Figure 19: Results of fifth comparison: bent-2d minus bent-3d.

- for 0–120 km. *Advances in Space Research*, 10(6), pp. 3–12, doi:10.1016/0273-1177(90)90230-W.
- Côté, J., S. Gravel, A. Méthot, A. Patoine, M. Roch, and A. Staniforth. 1998. The operational CMC–MRB Global Environmental Multiscale (GEM) model. Part I: Design considerations and formulation. *Monthly Weather Review*, 126(6), pp. 1373–1395, doi:10.1175/1520-0493(1998)126<1373:TOCMGE>2.0.CO;2.
- Dabberdt, W.F., R. Shellhorn, H. Cole, A. Paukkunen, J. Horhammer, and V. Antikainen. 2002. Radiosondes. In *Encyclopedia of Atmospheric Sciences*, eds. J.R. Holton, J.A. Curry, and J.A. Pyle, Academic Press, Oxford, ISBN 9780122270901, pp. 1900–1913, doi:10.1016/B0-12-227090-8/00344-4.
- Fleming, E.L., S. Chandra, M.R. Schoeberl, and J.J. Barnet. 1988. Monthly mean global climatology of temperature, wind, geopotential height and pressure for 0–120 km. Technical Memorandum 100697, NASA Goddard Space Flight Center, Greenbelt, Md., February, 91 pp., <http://hdl.handle.net/2060/19880013119>.
- Gardner, C.S. 1976. Effects of horizontal refractivity gradients on the accuracy of laser ranging to satellites. *Radio Science*, 11(12), pp. 1037–1044, doi:10.1029/RS011i012p01037.
- Ghoddousi-Fard, R., and P. Dare. 2007. A climatic based asymmetric mapping function using a dual radiosonde raytracing approach. *Proceedings of the 20th International Technical Meeting of the Satellite Division of the Institute of Navigation—ION GNSS 2007*, The Institute of Navigation, Fort Worth, Tex., September 25–28, pp. 2870–2879.
- Golding, B.W. 2002. Weather prediction: Regional prediction models. In *Encyclopedia of Atmospheric Sciences*, eds. J.R. Holton, J.A. Curry, and J.A. Pyle, Academic Press, Oxford, ISBN 9780122270901, pp. 2557–2562, doi:10.1016/B0-12-227090-8/00253-0.
- Hartmann, D.L. 2002. Climate: Overview. In *Encyclopedia of Atmospheric Sciences*, eds. J.R. Holton, J.A. Curry, and J.A. Pyle, Academic Press, Oxford, ISBN 9780122270901, pp. 403–411, doi:10.1016/B0-12-227090-8/00024-5.
- Hopfield, H.S. 1969. Two-quartic tropospheric refractivity profile for correcting satellite data. *Journal of Geophysical Research*, 74(18), pp. 4487–4499.
- Ifadis, I.M., and P. Savvaidis. 2001. Space to earth geodetic observations: approaching the atmospheric effect. *Physics and Chemistry of the Earth, Part A*, 26(3), pp. 195–200, doi:10.1016/S1464-1895(01)00046-1.
- Johnson, D.L., B.C. Roberts, and W.W. Vaughan. 2002. Reference and standard atmosphere models. *10th Conference on Aviation, Range, and Aerospace Meteorology*, Portland, Oreg., May 13–16. <http://hdl.handle.net/2060/20020092087>.
- Lorenc, A.C. 2002. Weather prediction: Data assimilation. In *Encyclopedia of Atmospheric Sciences*, eds. J.R. Holton, J.A. Curry, and J.A. Pyle, Academic Press, Oxford, ISBN 9780122270901, pp. 2542–2546, doi:10.1016/B0-12-227090-8/00458-9.
- McCarthy, D.D., and G. Petit (Eds.) 2004. IERS Conventions (2003). 127 pp., Frankfurt am Main: Verlag des Bundesamts für Kartographie und Geodäsie, Frankfurt, ISBN 3-89888-884-3, IERS Technical Note 32, <http://www.iers.org/MainDisp.csl?pid=46-25776>.
- Mendes, V.B. 1999. Modeling the Neutral-Atmosphere Propagation Delay in Radiometric Space Techniques. Ph.D. thesis, University of New Brunswick, Dept. of Geodesy and Geomatics Engineering, Fredericton, N.B., Canada, April, 349 pp., Technical Report 199, <http://gge.unb.ca/Pubs/TR199.pdf>.
- Nievinski, F.G. 2009. Ray-tracing options to mitigate the neutral atmosphere delay in GPS. Master's thesis, University of New Brunswick, Dept. of Geodesy and Geomatics Engineering, Fredericton, N.B., Canada, January, 232 pp., Technical Report 262, <http://hdl.handle.net/1882/1050>.
- Saastamoinen, J. 1972. Atmospheric correction for the troposphere and stratosphere in radio ranging of satellites. In *The Use of Artificial Satellites for Geodesy*, eds. S.W. Henriksen, A. Mancini, and B.H. Chovitz, Vol. 15 of *Geophysical Monograph Series*, American Geophysical Union, Washington, D.C., ISBN 0-87590-015-1, pp. 247–251.
- Thessin, R.N. 2005. Atmospheric signal delay affecting GPS measurements made by space vehicles during launch, orbit and reentry. Master's thesis, Massachusetts Institute of Technology, Dept. of Aeronautics and Astronautics, Cambridge, Mass., 182 pp., <http://hdl.handle.net/1721.1/33211>.
- Torge, W. 2001. *Geodesy*. 3rd ed., 416 pp., de Gruyter, Berlin, ISBN 978-3-11-017072-6, compl. rev. and extend. ed.
- Weisstein, E.W. 2008. Gaussian curvature. (Online), MathWorld—A Wolfram Web Resource. <http://mathworld.wolfram.com/GaussianCurvature.html>
- Young, A.T. 2006. Understanding astronomical refraction. *The Observatory*, Vol. 126, pp. 82–115, <http://adsabs.harvard.edu/abs/2006Obs...126...82>.

Authors

Felipe G. Nievinski is currently a doctoral student under the advice of Prof. Dr. Kristine M. Larson at the Department of Aerospace Engineering Sciences, University of Colorado at Boulder. He earned a MScE degree under the supervision of Prof. Dr. Marcelo C. Santos at the Department of Geodesy and Geomatics Engineering, University of New Brunswick, in 2009; and a degree in Geomatics Engineering from the Federal University of Rio Grande do Sul, Brazil, in 2005. He is a member of the American Geophysical Union and the Society for Industrial and Applied Mathematics.

Marcelo Santos is a Professor in the Department of Geodesy and Geomatics Engineering at the University of New Brunswick, Canada. He holds a M. Sc. Degree in Geophysics from the National Observatory, in Rio de Janeiro, and a Ph.D. Degree in Geodesy from the University of New Brunswick. He has been involved in research in the fields of Geodesy and GNSS. □